



**HAL**  
open science

## **Microbial life and biogeochemical cycling on land 3,220 million years ago**

Martin Homann, Pierre P Sansjofre, Mark van Zuilen, Christoph Heubeck, Jian Gong, Bryan Killingsworth, Ian Foster, Alessandro Airo, Martin van Kranendonk, Magali P Ader, et al.

► **To cite this version:**

Martin Homann, Pierre P Sansjofre, Mark van Zuilen, Christoph Heubeck, Jian Gong, et al.. Microbial life and biogeochemical cycling on land 3,220 million years ago. *Nature Geoscience*, 2018, 11 (9), pp.665 - 671. 10.1038/s41561-018-0190-9 . hal-01901955

**HAL Id: hal-01901955**

**<https://hal.univ-brest.fr/hal-01901955>**

Submitted on 21 Jan 2021

**HAL** is a multi-disciplinary open access archive for the deposit and dissemination of scientific research documents, whether they are published or not. The documents may come from teaching and research institutions in France or abroad, or from public or private research centers.

L'archive ouverte pluridisciplinaire **HAL**, est destinée au dépôt et à la diffusion de documents scientifiques de niveau recherche, publiés ou non, émanant des établissements d'enseignement et de recherche français ou étrangers, des laboratoires publics ou privés.

1 **Microbial life and biogeochemical cycling on land 3,220 million years ago**

2 Martin Homann<sup>1\*</sup>, Pierre Sansjofre<sup>1</sup>, Mark Van Zuilen<sup>2</sup>, Christoph Heubeck<sup>3</sup>, Jian Gong<sup>2</sup>,  
3 Bryan Killingsworth<sup>1</sup>, Ian S. Foster<sup>1</sup>, Alessandro Airo<sup>4</sup>, Martin J. Van Kranendonk<sup>5</sup>, Magali  
4 Ader<sup>3</sup>, and Stefan V. Lalonde<sup>1</sup>

5  
6 <sup>1</sup>European Institute for Marine Studies, CNRS-UMR6538 Laboratoire Géosciences Océan,  
7 Technopôle Brest-Iroise, Place Nicolas Copernic, 29280 Plouzané, France. \*corresponding author:  
8 [martin.homann@univ-brest.fr](mailto:martin.homann@univ-brest.fr)

9 <sup>2</sup>Institut de Physique du Globe de Paris, CNRS-UMR7154, 4 place Jussieu, 75005 Paris, France

10 <sup>3</sup>Department of Geosciences, Friedrich-Schiller-Universität, Burgweg 11, 07749 Jena, Germany

11 <sup>4</sup>Center of Astronomy and Astrophysics, Technische Universität Berlin, Straße des 17. Juni 136,  
12 10623 Berlin, Germany

13 <sup>5</sup>Australian Centre for Astrobiology, and School of Biological, Earth and Environmental Sciences,  
14 University of New South Wales, Sydney, NSW, 2052, Australia.

15  
16

17 **The colonization of emergent continental landmass by microbial life was an evolutionary**  
18 **step of paramount importance in Earth history. Here we report direct fossil evidence for**  
19 **life on land 3,220 Myr ago in the form of terrestrial microbial mats draping fluvial**  
20 **conglomerates and gravelly sandstones of the Moodies Group, South Africa. Combined**  
21 **field, petrographic, carbon isotope, and Raman spectroscopic analyses confirm the**  
22 **syndimentary origin and biogenicity of these unique fossil mats as well as their fluvial**  
23 **habitat. The carbon isotope composition of organic matter ( $\delta^{13}\text{C}_{\text{org}}$ ) from these mats**  
24 **define a narrow range centered on -21‰, in contrast to fossil mats of marine origin from**  
25 **nearby tidal deposits that show  $\delta^{13}\text{C}_{\text{org}}$  values as low as -34‰. Bulk nitrogen isotope**  
26 **compositions ( $2 < \delta^{15}\text{N} < 5\text{‰}$ ) are also significantly different from their marine counterparts**  
27 **( $0 < \delta^{15}\text{N} < 3\text{‰}$ ), which we interpret to reflect denitrification in the terrestrial habitat,**  
28 **possibly of an atmospheric source of nitrate. Our results support the antiquity of a**  
29 **thriving terrestrial biosphere during the Paleoproterozoic and suggest that a complex and**  
30 **microbially-driven redox landscape existed during the deposition of the Moodies Group,**  
31 **with distinct biogeochemical cycling occurring on land by 3,220 Myr ago.**

32  
33

34 While there is abundant evidence that microbial life thrived in the oceans as far back as there  
35 is a sedimentary record<sup>1-5</sup>, significantly less is known about microbial colonization of the land  
36 surface. Before 3,000 Myr ago, much of the Earth may have been submerged<sup>6</sup>, and accordingly,  
37 direct fossil evidence for terrestrial<sup>7</sup> life prior to the Mesoproterozoic is extremely rare<sup>8,9</sup>. It is also

38 inferential, largely derived from the study of paleosols as old as 3,200 Myr<sup>10–14</sup>. A suite of  
39 suggestive biosignatures in hot spring deposits indicate that life may have already been  
40 occupying terrestrial niches by 3,480 Myr<sup>15</sup>. Here we present the discovery of a new locality in  
41 the Paleoproterozoic Moodies Group, Barberton Greenstone Belt (BGB), South Africa, where  
42 exceptionally-preserved microbial mats are exposed in sediments of an ancient fluvial system.  
43 These terrestrial fossils represent a significant expansion of the known diversity of microbial  
44 life in the Moodies Group, which until now has been restricted solely to marine settings<sup>16–20</sup>.

45  
46 The Moodies Group is the uppermost of the three stratigraphic units constituting the Barberton  
47 Greenstone Belt (Supplementary Fig. 1) and represents the world's oldest well-preserved  
48 alluvial to shallow marine deposit<sup>21,22</sup>. It consists of a thick (up to 3.5 km) succession of alluvial  
49 to shallow-marine quartz-rich sandstones with subordinate conglomerates, mudstones, thin  
50 tuffs, banded iron formations, and a single basaltic lava<sup>22</sup>. The age of the Moodies Group is  
51 tightly constrained by several dacitic tuffs and rare felsic dikes radiating from the Kaap Valley  
52 tonalite that crosscut the Moodies Group along the northern margin of the BGB. U-Pb dating  
53 of single-zircons from these units indicate that deposition began about  $3,223 \pm 1$  Myr and had  
54 ended by about  $3,219 \pm 9$  Myr<sup>23,24</sup>. The southwestward-plunging Dycedale Syncline, approx. 2  
55 km east of Barberton, hosts a steeply dipping >350 m thick succession of Moodies Group  
56 conglomerates and cross-bedded sandstones. A large variety of sedimentary structures indicates  
57 that this succession records a transition from alluvial-fluvial (terrestrial) to tide-influenced  
58 marine sedimentation<sup>21,22</sup> (Supplementary Fig. 2).

59

### 60 **Terrestrial microbial mats in fluvial sandstones**

61 Our study is focused on fossilized microbial mats discovered in this unique terrestrial-to-marine  
62 transition in the Dycedale Syncline. The base of the section begins with a ~75-m-thick  
63 sedimentary unit including a ~40 m thick, polymict, mostly clast-supported conglomerate in

64 the central part (unit B of ref. 22; Supplementary Fig. 2). The poor sorting and angularity of  
65 clasts, poorly developed internal fabrics, clast imbrication, thin intercalated sandstone beds with  
66 upper-plane bed horizontal lamination, and the immature composition of this conglomerate  
67 indicate a proximal sediment source associated with episodic, short-lived, high-energy  
68 unidirectional transport. These fabrics and associations are typical for sheet flow-dominated  
69 alluvial fans and/or proximal braided streams with highly variable discharge. The conglomerate  
70 is under- and overlain by 10- and 25-m-thick (respectively) gravelly sandstones with  
71 carbonaceous laminations and minor interbedded conglomerate beds. These lens- or wedge-  
72 shaped beds are 0.2 to 2 m thick, commonly vertically stacked, and show minor channel incision  
73 from erosional downcutting, characteristic of fluvial deposition and transport (Fig. 1a). Pebble-  
74 to boulder-sized clasts (up to ~40 x 40 cm) are subrounded, poorly-sorted, and embedded in a  
75 quartz-rich coarse-sandy matrix (Fig. 1b). The transition to overlying gravelly, medium- to  
76 coarse-grained quartzofeldspathic sandstones is gradational. These horizontal to low-angle  
77 planar cross-bedded sandstones are locally interbedded with discontinuous mudstones with  
78 desiccation cracks, indicating periods of subaerial exposure (Supplementary Fig. 3). Overlying  
79 strata gradually deepen upward through deltaic, and medium-energy tidal, into subtidal  
80 siliciclastic deposits. The position of the conglomerate-bearing deposits at the base of this  
81 transgressive, fining- and deepening-upward sequence, and the absence of any sedimentary  
82 structure indicative of tidal or marine conditions, further suggests that the gravelly sandstones  
83 and conglomerates represent a terrestrial depositional environment, likely a fluvial coastal  
84 braidplain that was updip of an estuary<sup>22</sup>.

85

86 The wavy and crinkly carbonaceous laminations within these gravelly sandstones and on top of  
87 the conglomerate beds show a variety of features consistent with a biogenic origin. They are  
88 densely spaced at the mm-scale, and both onlap and drape protruding clasts (Fig. 1c-d). Laminae  
89 are bent upwards and plastically deformed by 10- to 50-cm-high subvertical fluid-escape

90 structures, indicating their cohesive water-impermeable nature and synsedimentary origin (Fig.  
91 1e, Supplementary Fig. 4). A high strength and cohesiveness of the laminae is further supported  
92 by their association with coarse-grained sandstone and conglomerate beds that were repeatedly  
93 emplaced on top of the laminae without severely damaging or eroding them (Fig. 2a). However,  
94 petrographic analysis also reveals that during periods of increased current velocity, and  
95 therefore higher shear stress, laminae were partially eroded, ripped up and reworked as  
96 fragments of up to several cm in length (Fig. 2a and 2c-f). In thin section, the 0.5 - 4 mm thick  
97 laminae are composed of a dense meshwork of interwoven filament-like microstructures that  
98 drape horizontally laminated and rippled sandstones, onlap individual clasts, and envelop  
99 “floating” detrital grains of fine-grained sand whose long axes are preferentially aligned parallel  
100 to bedding (Fig. 2a-b). Individual carbonaceous filamentous structures are 1 - 3  $\mu\text{m}$  in diameter  
101 and may exceed 100  $\mu\text{m}$  in length, commonly bundled and twisted around each other (Fig. 2c;  
102 Supplementary Fig. 5), consistent with, but not exclusive to, modern filamentous  
103 microorganisms forming biofilms. The excellent preservation of these features is thought to be  
104 due to a combination of very early silicification, low tectonic strain, and the low temperature  
105 of post-depositional hydrothermal overprinting ( $<150^\circ\text{C}$ ) in the interior part of the Barberton  
106 Greenstone Belt<sup>19,25</sup>. Raman microspectroscopy demonstrates that the carbonaceous laminae of  
107 both the terrestrial and marine mats<sup>19</sup> are composed of organic carbon that has experienced  
108 similar peak temperatures of  $\sim 365^\circ\text{C}$  (see Methods), consistent with the metamorphic grade of  
109 lower greenschist facies established by mineralogical indicators<sup>26</sup> and previous Raman-based  
110 estimates of regional peak metamorphic temperatures for the central part of the BGB<sup>27</sup> (Fig. 3,  
111 Supplementary Fig. 6, Supplementary Table 1). This confirms that the laminae are of  
112 syngenetic origin with the sandstone. Based on the combined evidence of carbonaceous  
113 composition, syngenicity, cohesiveness, sediment trapping behavior, and the presence of  
114 filamentous microstructures, the laminae are confidently identified as the fossilized remnants  
115 of microbial mats.

116 The presence of microbial mats on land during the Paleoproterozoic provides important insights  
117 into the timing of certain evolutionary innovations required for terrestrialization. The Archean  
118 land surface was likely a harsh environment subject to repeated desiccation, fluvial and/or  
119 aeolian abrasion, and presumably, intense UV radiation. Its colonization suggests that the  
120 terrestrial mats possessed a variety of adaptations, including tolerance to high shear stresses via  
121 formation of cohesive and resistive mats, production of hygroscopic EPS (extracellular  
122 polymeric substance) to maintain wetting during subaerial exposure, synthesis of UV-screening  
123 pigments and an enhanced capacity for DNA-repair to cope with cellular damage induced by  
124 desiccation and/or exposure to high-incidence UV radiation. It appears that terrestrial mats of  
125 the Moodies Group already possessed such coping mechanisms at 3,220 Myr.

126

127 Our new report of terrestrial mat fossils adds to the known diversity of the Moodies ecosystem,  
128 which includes large spheroidal microfossils<sup>16</sup>, widespread shallow marine tufted microbial  
129 mats with trapped gas bubbles<sup>17-19</sup>, and remnants of cavity-dwelling microbes thriving beneath  
130 the mats<sup>20</sup>. These coeval marine microbial communities are preserved in sandstones in the  
131 nearby Saddleback Syncline that show clear bidirectional paleocurrent patterns characteristic  
132 of deposition under tidal influence<sup>19</sup>.

133

134 To better characterize and distinguish the paleobiological context of these unique terrestrial  
135 mats from their marine counterparts, we subsampled mat-rich horizons from both and analyzed  
136 them for the carbon isotope composition of organic matter and for bulk nitrogen isotope  
137 composition. We also examined dolomite remnants that occur as bladed to blocky cement in  
138 mm- to cm-sized bedding-parallel cavities beneath the mats<sup>19,20</sup> in both environments. In places  
139 these carbonates are plastically deforming and rupture the mats, which further indicates their  
140 early diagenetic formation, prior to sandstone lithification (Supplementary Fig. 7). All  
141 carbonates yielded homogeneous mean  $\delta^{13}\text{C}_{\text{carb}}$  values of  $+0.2 \pm 0.2\text{‰}$  and  $\delta^{18}\text{O}_{\text{carb}}$  values of -

142 15.4‰ ±0.2‰ (n=16, Supplementary Table 2), common values for dolomitic carbonates of  
143 Archean age that rule out significant secondary exchange between carbon pools after burial.

144

#### 145 **Carbon fixation in Moodies Group microbial mats**

146 The carbon isotope composition of preserved organic matter provides a more direct link to  
147 metabolic activity during mat growth. In the terrestrial mats,  $\delta^{13}\text{C}_{\text{org}}$  values range between -  
148 23.6‰ and -17.9‰, with a mean of -21.2‰ (n=36; Supplementary Table 3). These values  
149 contrast with isotopically lighter  $\delta^{13}\text{C}_{\text{org}}$  values of microbial communities from the coeval  
150 marine deposits, ranging between -33.9‰ and -21.3‰, with a mean of -27.4 (n=30; Fig. 4).  
151 The observed difference between the two data sets is statistically significant (two-tailed  
152 Welsh's t-test,  $p < 0.0001$ ). The ~6‰ shift to heavier  $\delta^{13}\text{C}_{\text{org}}$  values in the terrestrial realm thus  
153 suggests significant environmental and metabolic diversity across this Paleoarchean ecosystem  
154 landscape.

155

156 There are several non-mutually exclusive explanations for this shift. Firstly, cell size, growth  
157 rate, and species-specific differences in  $\text{CO}_2$  diffusion rates all influence  $\epsilon_p$ , the carbon isotopic  
158 fractionation factor associated with phototrophic carbon fixation<sup>28,29</sup>. However, the influence  
159 of these factors on  $\epsilon_p$  tends toward zero<sup>29</sup> as  $p\text{CO}_2$  approaches the elevated values inferred for  
160 the Archean<sup>30</sup>, and some bacterial species exhibit little variation even at low  $\text{CO}_2$   
161 concentrations<sup>31</sup>. A more likely explanation for this shift is a mixing of carbon sources with  
162 different isotopic compositions. The terrestrial samples exhibit a narrow distribution in  $\delta^{13}\text{C}_{\text{org}}$   
163 values, suggesting a relatively homogenous source centered around -21‰. This  $\delta^{13}\text{C}_{\text{org}}$   
164 composition is consistent with autotrophic carbon fixation via the Calvin-Benson cycle<sup>32,33</sup>,  
165 whether by oxygenic or anoxygenic phototrophs. Marine samples reach values that are  
166 isotopically as heavy, yet cover a larger spread extending to lighter  $\delta^{13}\text{C}_{\text{org}}$  values, some as low

167 as -34‰. These features suggest that in the marine realm, mixing occurred between material  
168 with the same isotopic composition (-21‰) as terrestrial samples and material with carbon that  
169 was isotopically lighter than -34‰. Under high pCO<sub>2</sub>, carbon fixed by the Calvin-Benson cycle  
170 is unlikely to reach such low values<sup>34</sup>, which are best explained instead by biomass derived  
171 from other carbon fixation pathways, notably the reductive Acetyl Co-A (Wood-Ljungdahl)  
172 pathway<sup>34-36</sup>. This includes acetogenic bacteria, methanogens, and sulfate reducers that, with  
173 the exception of some examples of the latter<sup>37</sup>, are obligate anaerobes. The terrestrial mat  
174 samples are rather remarkable in that the light carbon isotope signature that should be associated  
175 with alternative fixation pathways such as the reductive Acetyl Co-A pathway is not observed.

176

177 We suggest that this disparity reflects differences in fermentative or respiratory processes  
178 occurring in the mats along a paleoenvironmental transect. One possibility is that higher  
179 sedimentation rates in the terrestrial realm promoted rapid burial of carbon formed at the mat  
180 surface via the Calvin-Benson pathway, while lower sedimentation rates in marine settings  
181 permitted greater expression of the anaerobic reductive Acetyl-CoA pathway at depth in the  
182 mat. A related possibility is that distinct microbial communities inhabited these different  
183 environments. Indeed, in modern microbial mats, production of CH<sub>4</sub> is independent of diel  
184 cycling between ambient oxic and anoxic water conditions, yet appears strongly suppressed in  
185 intertidal mats and enhanced in subtidal mats as the result of differences in their anaerobic  
186 community structure at depth<sup>38</sup>. These include differences in the activity of sulphate reducers,  
187 who outcompete methanogens for organic substrates even at sulphate concentrations as low as  
188 60 μM<sup>39</sup>. The local presence of sulphate in supratidal to braided-fluvial environments during  
189 Moodies Group deposition is indicated by common pseudomorphic relics of gypsum<sup>40</sup> and  
190 isotopic evidence for sulphate reduction in Moodies Group paleosols<sup>14</sup>. However, other  
191 possibilities exist that may have resulted in a greater contribution of carbon from pathways  
192 other than Calvin-Benson, such as the Wood-Ljungdahl pathway, in the marine realm. It has



193 been suggested that hydrogen gas was the principal electron donor for photosynthetic mat  
194 growth in the 3,416 Myr Buck Reef Chert (Onverwacht Group, also in the BGB)<sup>3,41</sup>.  
195 Anoxygenic phototrophs growing on hydrogen using the reverse tricarboxylic acid or 3-  
196 hydroxypropionate CO<sub>2</sub> fixation pathways are characterized by carbon isotope compositions  
197 that tend to be heavier than -14‰ (see review in ref. 36 and references therein), for which no  
198 evidence is observed in our dataset. However, if locally abundant, hydrogen might have been  
199 important in stimulating anaerobic metabolism via the Wood-Ljungdahl pathway. Both  
200 oxygenic and anoxygenic phototrophs may themselves produce significant quantities of  
201 hydrogen gas via bi-directional hydrogenases, and under conditions of nitrogen limitation, this  
202 may also occur via a nitrogenase-catalyzed side reaction<sup>42</sup>. In the terrestrial realm, rapid burial,  
203 the increased availability of sulphate and/or fixed nitrogen, and a depressed role for hydrogen,  
204 are all plausible explanations for the contrasting carbon pools preserved in the mats, however  
205 it is difficult to draw further inference based on carbon isotope data alone.

206

### 207 **Isotopic insight into nitrogen cycling 3,220 Myr ago**

208 Bulk nitrogen isotopic compositions of mat samples also record a significant contrast between  
209 the two paleoenvironments that points to differences in mat community structure and  
210 respiratory processes.  $\delta^{15}\text{N}$  values of marine mats range between -0.7‰ and +3.1‰, with an  
211 average of +1.8‰ (n=10), in contrast to terrestrial  $\delta^{15}\text{N}$  values that are generally more positive,  
212 ranging between +1.9‰ and +5.6‰ with a mean of +4.3‰ (n=10, Fig. 4, Supplementary Table  
213 4). The  $\delta^{15}\text{N}$  values of the two sample sets are statistically different, even if the two marine data  
214 points that are lowest in  $\delta^{15}\text{N}$  are considered as outliers (two-tailed Welch's t-test,  $p < 0.002$ ).  
215 While the marine samples show near-zero values consistent with atmospheric nitrogen fixation,  
216 values of up to +5‰ in the terrestrial samples are outside the range of typical fractionations  
217 associated with growth on atmospheric N<sub>2</sub>. C/N ratios range from 8 to 60 and show no  
218 covariation with  $\delta^{15}\text{N}$  values; similar to peak metamorphic temperatures determined by Raman

219 spectroscopy (Supplementary Table 1), C/N ratios show no significant differences between  
220 terrestrial and marine mat samples (Supplementary Figure 8), suggesting that the differences  
221 observed in  $\delta^{15}\text{N}$  are not the expression of different diagenetic or metamorphic histories (e.g.,  
222 ref. 34). Moreover, it has been shown that  $\delta^{15}\text{N}$  values are resistant to modification during low  
223 grade metamorphism<sup>43</sup>, in the case of kerogen varying no more than 1‰ for sediments reaching  
224 greenschist facies<sup>44</sup>. The lowest C/N ratios observed are probably linked to the presence of clay  
225 minerals that retain nitrogen produced during diagenesis. Total nitrogen contents (12–64 ppm,  
226 Supplementary Table 4) show no significant differences between marine and terrigenous  
227 sediments, and show no relation to clay content (~17 to 32% illite and muscovite in samples  
228 for which X-ray diffraction was performed), suggesting that variable contributions of nitrogen  
229 bound to clay, including allochthonous clay, cannot explain the isotopic contrast between the  
230 two datasets, which are instead most likely recording different primary compositions of mat  
231 biomass.

232

233 Three different biological mechanisms are known to produce biomass with  $\delta^{15}\text{N}$  compositions  
234 greater than +2‰ (see ref. 45 for a detailed discussion). The first, and the only mechanism  
235 possible in the absence of oxidative nitrogen cycling, is partial assimilation of  $\text{NH}_4^+$ , whereby  
236 preferential uptake of  $^{14}\text{NH}_4^+$  can drive the residual  $\text{NH}_4^+$  toward isotopically heavier values  
237 (e.g., ref. 46). However, only after most of the  $\text{NH}_4^+$  pool has been assimilated would residual  
238  $\text{NH}_4^+$  achieve values as heavy as +5‰ and we see no evidence in our dataset for light isotope  
239 enrichments that would indicate this process. The two remaining hypotheses are partial  
240 nitrification and/or partial denitrification, both of which require oxidative nitrogen cycling in  
241 the terrestrial mats. Partial nitrification requires a local source of  $\text{O}_2$  (with or without Mn oxide  
242 intermediates) and has only been observed to generate such positive values in stratified water  
243 bodies where  $\text{O}_2$  concentrations are highly dynamic as the result of seasonal overturning<sup>45</sup>,  
244 which does not apply to the fluvial setting of the terrestrial mats. Finally, partial denitrification

245 of a stable nitrate pool is the process that is most commonly evoked for the generation of  
246 isotopically heavy  $\delta^{15}\text{N}$  compositions in organic matter<sup>43,45</sup>, and would also appear to be the  
247 most parsimonious explanation for the isotopically heavy  $\delta^{15}\text{N}$  compositions of the terrestrial  
248 mats.

249

250 The source of nitrate to the terrestrial mat ecosystem may have been atmospheric. Prebiotic  
251 generation of fixed nitrogen ( $\text{NO}^-$ ,  $\text{NO}_2^-$ , and  $\text{NO}_3^-$ ) in the atmosphere by lightning discharge at  
252  $p\text{O}_2 < 10^{-5}$  present atmospheric level (PAL) is estimated to be around 2 to 4 x  $10^{11}$  g N per  
253 year<sup>47,48</sup>, which translates to a global surface flux of 0.1 to 0.2  $\mu\text{g N m}^{-2} \text{ day}^{-1}$ . While this flux  
254 may have been too diffuse to be a significant source of fixed nitrogen to the marine biosphere<sup>49</sup>,  
255 fluvial mats would have had access to fixed nitrogen that is integrated over a larger area by  
256 surface runoff. We calculate the drainage area required to supply an atmospheric fixed nitrogen  
257 flux to mats at a rate that is comparable to that of nitrogen fixation by modern intertidal  
258 microbial mats (6 to 79  $\text{mg N m}^{-2} \text{ day}^{-1}$ )<sup>50</sup> to be only 0.02 to 0.62  $\text{km}^2$ . In other words, rainout  
259 of fixed nitrogen onto the early land surface should have had a profound influence on nitrogen  
260 cycling in early terrestrial ecosystems, one that appears expressed in the contrasting nitrogen  
261 isotope compositions of microbial mat biomass between terrestrial and marine settings in the  
262 Moodies Group.

263

264 Our observations rejoin those from the slightly younger (~3,000 Myr) Mesoarchean fluvio-  
265 lacustrine Lalla Rookh sandstone (W. Australia) where a contrast in the carbon isotope  
266 composition of organic matter has also been observed<sup>34</sup>, albeit relative to marine sediments of  
267 similar age from other localities, whereas our comparison is made on approximately coeval  
268 sediments from the same basin. In the Lalla Rookh sandstone, the carbon isotopic contrast  
269 occurred in the reverse sense (with more important  $\delta^{13}\text{C}$  depletion in lacustrine sediments) and

270 without any evidence for oxidative nitrogen cycling. Nonetheless, the ensemble of emerging  
271 evidence indicates that microbial communities already inhabited terrestrial surface  
272 environments, and fundamentally differed from their marine counterparts in their  
273 biogeochemical cycling of carbon and nitrogen, at the dawn of continental emergence ca. 3,220  
274 Myr ago.

275 **References**

- 276 1. Nutman, A. P., Bennett, V. C., Friend, C. R. L., Van Kranendonk, M. J. & Chivas, A.  
 277 R. Rapid emergence of life shown by discovery of 3,700-million-year-old microbial  
 278 structures. *Nature* **537**, 535–538 (2016).
- 279 2. Allwood, A. C., Walter, M. R., Kamber, B. S., Marshall, C. P. & Burch, I. W.  
 280 Stromatolite reef from the Early Archaean era of Australia. *Nature* **441**, 714–718  
 281 (2006).
- 282 3. Tice, M. M. & Lowe, D. R. Photosynthetic microbial mats in the 3,416-Myr-old  
 283 ocean. *Nature* **431**, 549–552 (2004).
- 284 4. Wacey, D., Kilburn, M. R., Saunders, M., Cliff, J. & Brasier, M. D. Microfossils of  
 285 sulphur-metabolizing cells in 3.4-billion-year-old rocks of Western Australia. *Nat.*  
 286 *Geosci.* **4**, 698–702 (2011).
- 287 5. Dodd, M. S. *et al.* Evidence for early life in Earth’s oldest hydrothermal vent  
 288 precipitates. *Nature* **543**, 60–64 (2017).
- 289 6. Flament, N., Coltice, N. & Rey, P. F. The evolution of the <sup>87</sup>Sr/<sup>86</sup>Sr of marine  
 290 carbonates does not constrain continental growth. *Precambrian Res.* **229**, 177–188  
 291 (2013).
- 292 7. The term “terrestrial” has multiple definitions; here we follow convention from  
 293 literature on the Precambrian biosphere by considering any life on the emerged  
 294 continental surface, aquatic or subaerial, as terrestrial (see supplementary text).
- 295 8. Beraldi-Campesi, H. Early life on land and the first terrestrial ecosystems. *Ecol.*  
 296 *Process.* **2**, 1 (2013).
- 297 9. Wellman, C. H. & Strother, P. K. The terrestrial biota prior to the origin of land plants  
 298 (embryophytes): a review of the evidence. *Palaeontology* **58**, 601–627 (2015).
- 299 10. Watanabe, Y., Martini, J. E. & Ohmoto, H. Geochemical evidence for terrestrial  
 300 ecosystems 2.6 billion years ago. *Nature* **408**, 574–578 (2000).
- 301 11. Rye, R. & Holland, H. D. Life associated with a 2.76 Ga ephemeral pond?: Evidence  
 302 from Mount Roe #2 paleosol. *Geology* **28**, 483–486 (2000).
- 303 12. Crowe, S. A. *et al.* Atmospheric oxygenation three billion years ago. *Nature* **501**, 535–  
 304 8 (2013).
- 305 13. Mukhopadhyay, J. *et al.* Oxygenation of the Archean atmosphere: New paleosol  
 306 constraints from eastern India. *Geology* **42**, 923–926 (2014).
- 307 14. Nabhan, S., Wiedenbeck, M., Milke, R. & Heubeck, C. Biogenic overgrowth on  
 308 detrital pyrite in ca. 3.2 Ga Archean paleosols. *Geology* **44**, 763–766 (2016).
- 309 15. Djokic, T., Van Kranendonk, M. J., Campbell, K. A., Walter, M. R. & Ward, C. R.  
 310 Earliest signs of life on land preserved in ca. 3.5 Ga hot spring deposits. *Nat. Commun.*  
 311 **8**, 1–8 (2017).
- 312 16. Javaux, E. J., Marshall, C. P. & Bekker, A. Organic-walled microfossils in 3.2-billion-  
 313 year-old shallow-marine siliciclastic deposits. *Nature* **463**, 934–8 (2010).
- 314 17. Noffke, N., Eriksson, K. A., Hazen, R. M. & Simpson, E. L. A new window into Early  
 315 Archean life: Microbial mats in Earth’s oldest siliciclastic tidal deposits (3.2 Ga  
 316 Moodies Group, South Africa). *Geology* **34**, 253 (2006).
- 317 18. Heubeck, C. An early ecosystem of Archean tidal microbial mats (Moodies Group,  
 318 South Africa, ca. 3.2 Ga). *Geology* **37**, 931–934 (2009).
- 319 19. Homann, M., Heubeck, C., Airo, A. & Tice, M. M. Morphological adaptations of 3.22  
 320 Ga-old tufted microbial mats to Archean coastal habitats (Moodies Group, Barberton  
 321 Greenstone Belt, South Africa). *Precambrian Res.* **266**, 47–64 (2015).
- 322 20. Homann, M. *et al.* Evidence for cavity-dwelling microbial life in 3.22 Ga tidal  
 323 deposits. *Geology* **44**, 51–54 (2016).
- 324 21. Eriksson, K. A., Simpson, E. L. & Mueller, W. U. An unusual fluvial to tidal transition

- 325 in the mesoarchean Moodies Group, South Africa: A response to high tidal range and  
 326 active tectonics. *Sediment. Geol.* **190**, 13–24 (2006).
- 327 22. Heubeck, C. *et al.* Geological constraints on Archean (3.22 Ga) coastal-zone processes  
 328 from the Dycedale Syncline, Barberton Greenstone Belt. *South African J. Geol.* **119**,  
 329 495–518 (2016).
- 330 23. De Ronde, C. E. J. & Kamo, S. L. An Archaean arc-arc collisional event: A short-lived  
 331 (ca 3 Myr) episode, Weltevreden area, Barberton greenstone belt, South Africa. *J.*  
 332 *African Earth Sci.* **30**, 219–248 (2000).
- 333 24. Heubeck, C. *et al.* Timing of deposition and deformation of the Moodies Group  
 334 (Barberton Greenstone Belt, South Africa): Very-high-resolution of Archaean surface  
 335 processes. *Precambrian Res.* **231**, 236–262 (2013).
- 336 25. Farber, K., Dziggel, A., Trumbull, R. B., Meyer, F. M. & Wiedenbeck, M. Tourmaline  
 337 B-isotopes as tracers of fluid sources in silicified Palaeoarchean oceanic crust of the  
 338 Mendon Formation, Barberton greenstone belt, South Africa. *Chem. Geol.* **417**, 134–  
 339 147 (2015).
- 340 26. Xie, X., Byerly, G. R. & Ferrell Jr., R. E. Ilb trioctahedral chlorite from the Barberton  
 341 greenstone belt: crystal structure and rock composition constraints with implications to  
 342 geothermometry. *Contrib. to Mineral. Petrol.* **126**, 275–291 (1997).
- 343 27. Tice, M. M., Bostick, B. C. & Lowe, D. R. Thermal history of the 3.5–3.2 Ga  
 344 Onverwacht and Fig Tree Groups, Barberton greenstone belt, South Africa, inferred by  
 345 Raman microspectroscopy of carbonaceous material. *Geology* **32**, 37 (2004).
- 346 28. Popp, B. N. *et al.* Effect of Phytoplankton Cell Geometry on Carbon Isotopic  
 347 Fractionation. *Geochim. Cosmochim. Acta* **62**, 69–77 (1998).
- 348 29. Hayes, J. M., Strauss, H. & Kaufman, A. J. The abundance of in marine organic matter  
 349 and isotopic fractionation in the global biogeochemical cycle of carbon during the past  
 350 800 Ma. *Chem. Geol.* **161**, 103–125 (1999).
- 351 30. Driese, S. G. *et al.* Neoproterozoic paleoweathering of tonalite and metabasalt:  
 352 Implications for reconstructions of 2.69Ga early terrestrial ecosystems and  
 353 paleoatmospheric chemistry. *Precambrian Res.* **189**, 1–17 (2011).
- 354 31. Laws, E. A., Popp, B. N., Cassas, N. & Tanimoto, J. <sup>13</sup>C discrimination patterns in  
 355 oceanic phytoplankton: likely influence of CO<sub>2</sub> concentrating mechanisms, and  
 356 implications for palaeoreconstructions. *Funct. plant Biol.* **29**, 323–333 (2002).
- 357 32. Schidlowski, M. A 3,800-million-year isotopic record of life from carbon in  
 358 sedimentary rocks. *Nature* **333**, 313–318 (1988).
- 359 33. Eigenbrode, J. L. & Freeman, K. H. Late Archean rise of aerobic microbial ecosystems.  
 360 *Proc. Natl. Acad. Sci.* **103**, 15759–15764 (2006).
- 361 34. Stüeken, E. E. & Buick, R. Environmental control on microbial diversification and  
 362 methane production in the Mesoarchean. *Precambrian Res.* **304**, 64–72 (2018).
- 363 35. Slotznick, S. P. & Fischer, W. W. Examining Archean methanotrophy. *Earth Planet.*  
 364 *Sci. Lett.* **441**, 52–59 (2016).
- 365 36. Havig, J. R., Hamilton, T. L., Bachan, A. & Kump, L. R. Sulfur and carbon isotopic  
 366 evidence for metabolic pathway evolution and a four-stepped Earth system progression  
 367 across the Archean and Paleoproterozoic. *Earth-Science Rev.* **174**, 1–21 (2017).
- 368 37. Baumgartner, L. K. *et al.* Sulfate reducing bacteria in microbial mats: Changing  
 369 paradigms, new discoveries. *Sediment. Geol.* **185**, 131–145 (2006).
- 370 38. Hoehler, T. M., Bebout, B. M. & Des Marais, D. J. The role of microbial mats in the  
 371 production of reduced gases on the early Earth. *Nature* **412**, 324–327 (2001).
- 372 39. Lovley, D. R. & Klug, M. J. Sulfate reducers can outcompete methanogens at  
 373 freshwater sulfate concentrations. *Appl. Environ. Microbiol.* **45**, 187–92 (1983).
- 374 40. Nabhan, S., Lubber, T., Scheffler, F. & Heubeck, C. Climatic and geochemical  
 375 implications of Archean pedogenic gypsum in the Moodies Group (~3.2Ga), Barberton

- 376 Greenstone Belt, South Africa. *Precambrian Res.* **275**, 119–134 (2016).
- 377 41. Tice, M. M. & Lowe, D. R. Hydrogen-based carbon fixation in the earliest known  
378 photosynthetic organisms. *Geology* **34**, 37 (2006).
- 379 42. Bandyopadhyay, A., Stöckel, J., Min, H., Sherman, L. A. & Pakrasi, H. B. High rates  
380 of photobiological H<sub>2</sub> production by a cyanobacterium under aerobic conditions. *Nat.*  
381 *Commun.* **1**, 139 (2010).
- 382 43. Ader, M. *et al.* Interpretation of the nitrogen isotopic composition of Precambrian  
383 sedimentary rocks: Assumptions and perspectives. *Chem. Geol.* **429**, 93–110 (2016).
- 384 44. Ader, M. *et al.* Nitrogen isotopic evolution of carbonaceous matter during  
385 metamorphism: Methodology and preliminary results. *Chem. Geol.* **232**, 152–169  
386 (2006).
- 387 45. Stüeken, E. E. A test of the nitrogen-limitation hypothesis for retarded eukaryote  
388 radiation: Nitrogen isotopes across a Mesoproterozoic basinal profile. *Geochim.*  
389 *Cosmochim. Acta* **120**, 121–139 (2013).
- 390 46. Papineau, D. *et al.* High primary productivity and nitrogen cycling after the  
391 Paleoproterozoic phosphogenic event in the Aravalli Supergroup, India. *Precambrian*  
392 *Res.* **171**, 37–56 (2009).
- 393 47. Kasting, J. F. & Walker, J. C. G. Limits on oxygen concentration in the prebiological  
394 atmosphere and the rate of abiotic fixation of nitrogen. *J. Geophys. Res.* **86**, 1147  
395 (1981).
- 396 48. Navarro-gonz, R., Molina, M. J. & Molina, L. T. Nitrogen fixation by volcanic  
397 lightning in the early Earth. *Geophys. Res. Lett.* **25**, 3123–3126 (1998).
- 398 49. Stüeken, E. E., Kipp, M. A., Koehler, M. C. & Buick, R. The evolution of Earth's  
399 biogeochemical nitrogen cycle. *Earth-Science Rev.* **160**, 220–239 (2016).
- 400 50. Joye, S. B. & Paerl, H. W. Nitrogen Cycling In Microbial Mats - Rates And Patterns Of  
401 Denitrification And Nitrogen-Fixation. *Mar. Biol.* **119**, 285–295 (1994).

402  
403

#### 404 **Corresponding author**

405 Correspondence and request for materials should be addressed to M.H.

406 (martin.homann@univ-brest.fr)

407

#### 408 **Acknowledgements**

409 This work was supported by Deutsche Forschungsgemeinschaft (DFG) grant He2418/13–1,  
410 LabexMER ANR-10-LABX-19, and Prestige COFUND-GA-2013-609102. We thank N. and  
411 D. Oosthuizen for access to the private Mountainlands nature reserve, S. Bläsing and M. Grund  
412 for assistance with sample collection, J.-P. Oldra for thin section preparation, and O. Lebeau,  
413 C. Tanvet, C. Liorzou, M.-L. Rouget, and B. Gueguen for assistance with isotopic and  
414 elemental analysis.

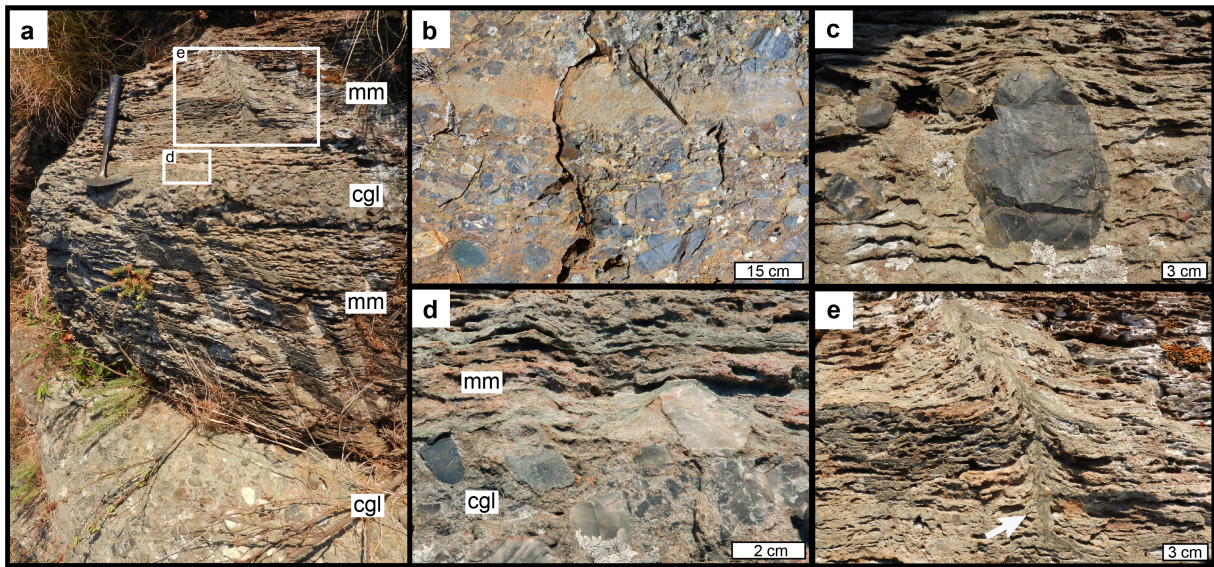
415

416 **Author contributions**

417 M.H. and C.H. carried out field work and collected samples in South Africa. P.S., M.A., and  
418 S.V.L. helped with the acquisition and interpretation of elemental and isotopic data. M.V.Z.  
419 and J.G. performed Raman analysis. B.K., I.S.F., A.A. and M.J.V.K. contributed to the  
420 discussion of the data. M.H. wrote the manuscript with significant contributions from all co-  
421 authors.

422

423 **Figures**

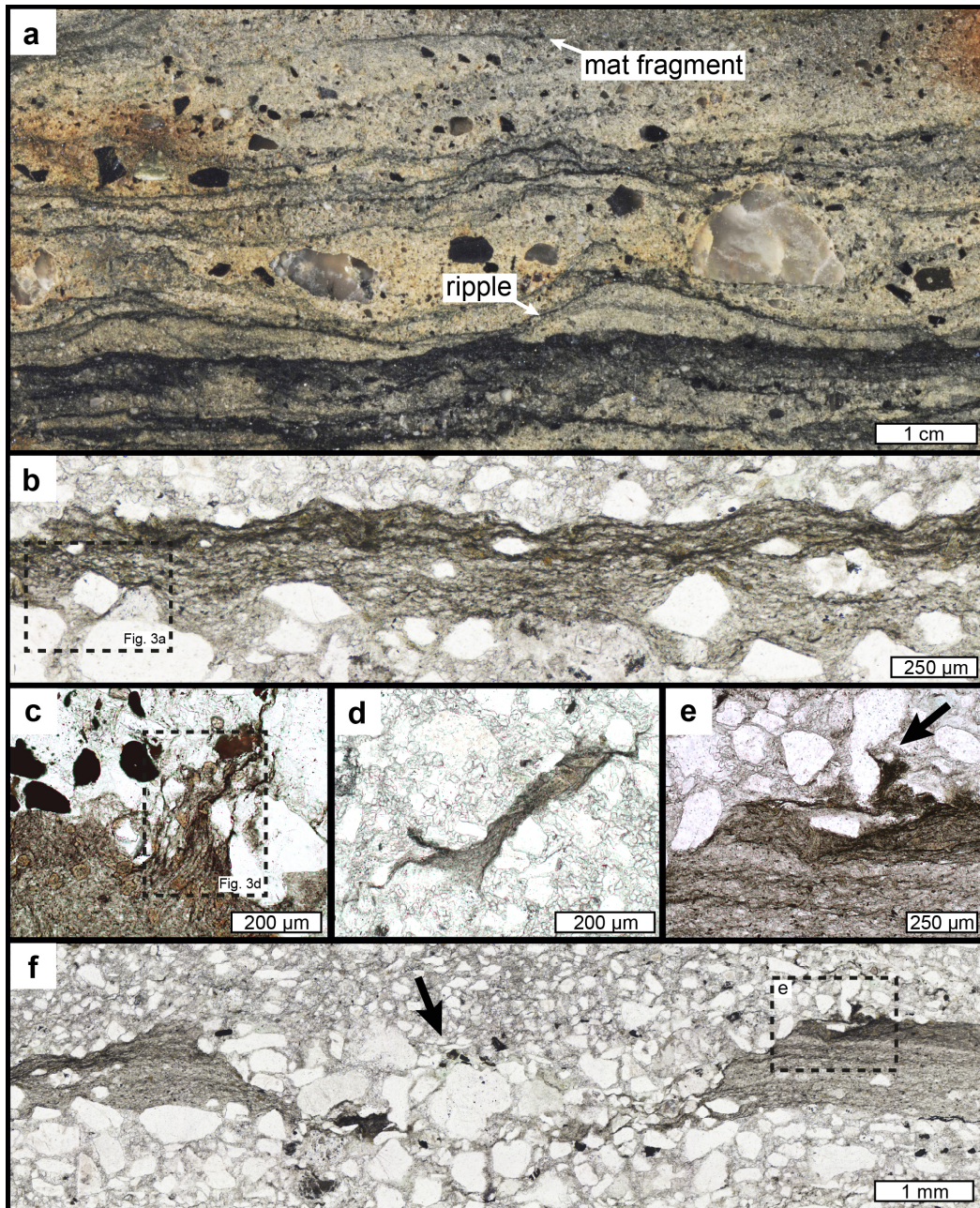


424

425

426 **Figure 1. Field photographs of fluvial sandstones and conglomerates hosting fossil**  
427 **terrestrial mats from the 3,220 Myr old Moodies Group. a**, Overview photograph showing  
428 interbedded fossil microbial mats (mm) and conglomerates (cgl). **b**, Mat-associated fluvial  
429 conglomerate, composed of subrounded pebbles and cobbles. **c, d**, Microbial mats draping and  
430 onlapping interbedded clasts within the sandstones and on top of conglomerate beds (close-up  
431 view of the framed area in (a)). **e**, Fluid-escape structure with well-defined central channel  
432 (arrow) that vertically disrupts the densely mat-laminated sandstone (close-up view of the  
433 framed area in (a)).





434

435 **Figure 2. Reflected and transmitted light photomicrographs of the terrestrial microbial**

436 **mats of the Moodies Group. a,** Dark carbonaceous laminae of the fossil mats draping

437 horizontally laminated and rippled sand and onlapping pebbles. Chips of eroded mat fragments

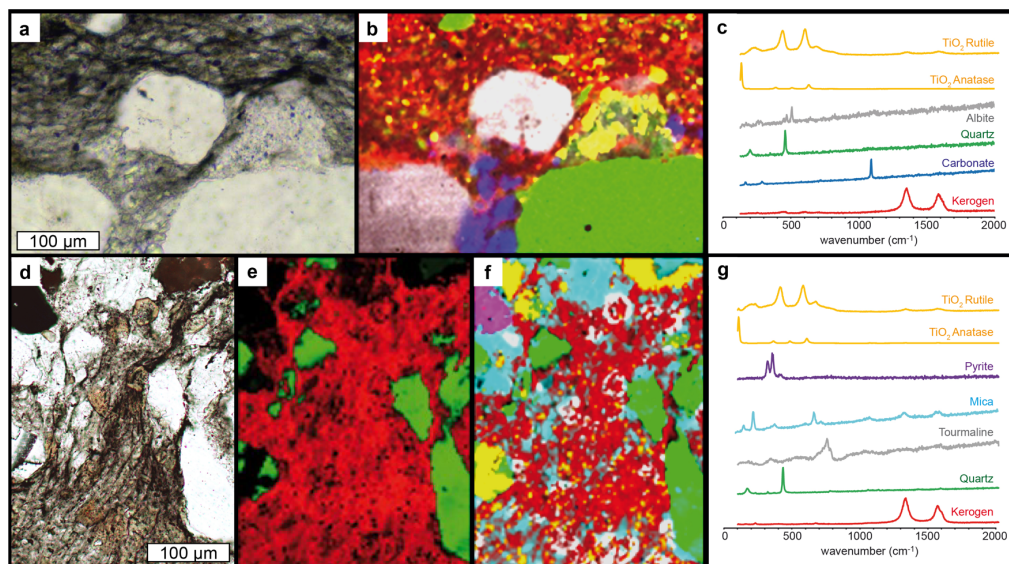
438 are preserved in cross-laminated, granular sandstone. **b,** Dense meshwork of interwoven

439 filamentous microstructures with trapped detrital grains. **c,** Bundled filamentous structures in

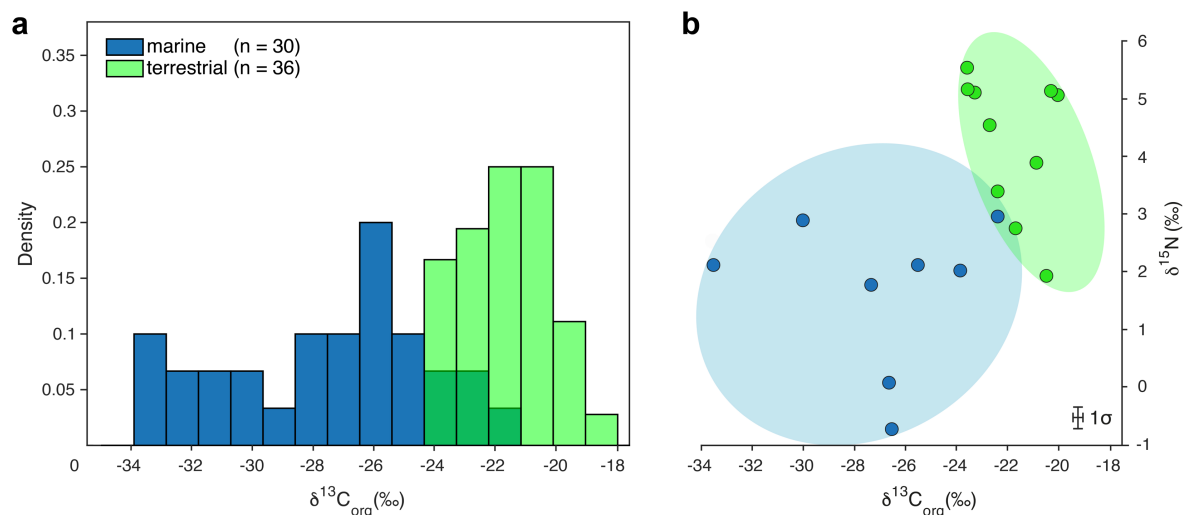
440 upper part of the mat. **d,** Close-up view of eroded mat fragment. **e,** Partially eroded microbial

441 mat laminae due to abrasion by impacting sand grains (arrow) and **f,** Erosional truncation of the

442 mat by small channel (arrow).



443  
 444 **Figure 3. Transmitted light photomicrographs of preserved kerogenous laminae (a) and**  
 445 **filamentous microstructures (d) of the terrestrial mats, with corresponding Raman**  
 446 **component maps for mineral phases and G-peak intensity for kerogenous phases (b, e, f), and**  
 447 **representative Raman component spectra (c, g). Note that the analyzed areas are close-up views**  
 448 **of the samples shown in Figure 2B and 2C, respectively.**  
 449



450  
 451 **Figure 4. Carbon isotope composition of organic matter and bulk nitrogen isotope**  
 452 **composition from terrestrial (green) and marine (blue) microbial mats of the**  
 453 **Paleoarchean Moodies Group. a, Histogram of organic carbon  $\delta^{13}\text{C}_{\text{org}}$  and b,  $\delta^{13}\text{C}_{\text{org}}$**   
 454 **versus  $\delta^{15}\text{N}$  values for both environments.**

455 **Methods**

456 **Optical microscopy.** Standard 30- $\mu\text{m}$ -thick, polished thin sections, oriented perpendicular to  
457 bedding, were analyzed using an Olympus BX60 petrographic microscope and a Zeiss Axio  
458 Scope.A1 equipped with a 63x oil objective lens. High resolution scans of entire thin sections  
459 were performed with a Zeiss Axio Zoom v16 motorized stereo microscope at the IPGP, Paris.

460

461 **Raman spectroscopy.** Raman analyses were performed using a Renishaw InVia Raman  
462 microscope coupled to an Olympus BX61 Confocal microscope, within the PARI analytical  
463 platform at the IPGP in Paris. Measurements were made with a 514 nm-excitation (Ar-ion laser)  
464 and adjusted to an on-sample intensity of 0.2 mW with a spot size of  $< 2 \mu\text{m}$  (50x objective).  
465 Beam centering and Raman spectral calibration were performed on a pure silicon chip with a  
466 specific Raman band at  $520.4 \text{ cm}^{-1}$ . All spectra were detected using 1800 l/mm grating, and a  
467 detector configuration in streamspot mode, providing a spectral range of  $2000 \text{ cm}^{-1}$  in static  
468 mode. Individual spot analyses were obtained in both static mode (2 x 20 s exposure, centered  
469 at  $1150 \text{ cm}^{-1}$  with a spectral range of  $100\text{-}2000 \text{ cm}^{-1}$ ) and extended mode (1 x 20 s exposure,  
470 spectral range  $100\text{-}4000 \text{ cm}^{-1}$ ). In order to determine Raman spectral indicators of the  
471 carbonaceous fractions, the individual spectra were truncated to  $900\text{-}1900 \text{ cm}^{-1}$ , and a linear  
472 background subtraction was performed, using the program Wire 2.0. Peak-decomposition was  
473 performed using two generally reported methods: a) a 2-peak fit, assigning a D-peak at ca.  $1350$   
474  $\text{cm}^{-1}$  and a G-peak at ca.  $1600 \text{ cm}^{-1}$  (following the procedure outlined in Sforza et al.<sup>51</sup>), b) a 4-  
475 peak fit, assigning a D1-, D2-, D3-, and G-peak at ca.  $1350 \text{ cm}^{-1}$ ,  $1620 \text{ cm}^{-1}$ ,  $1500 \text{ cm}^{-1}$ , and  
476  $1600 \text{ cm}^{-1}$ , respectively (following the procedure outlined in Sforza et al.<sup>51</sup>, Supplementary Fig.  
477 6). In all obtained spectra a D4-peak at ca.  $1200 \text{ cm}^{-1}$  was absent and was therefore not assigned  
478 during the peak decomposition procedure. Spectral data of the decomposed peaks (position,  
479 width, height, area) were recorded and used for calculating the Raman indicators D-FWHM (D-  
480 peak full width at half maximum) and ID/IG (height-based D/G) using the 2-peak fit, and D1-

481 FWHM, R1 (height-based D1/G) and R2 (area-based D1/D1+D2+G) using the 4-peak fit. Two  
482 geothermometers could then be calculated, that of Beyssac et al.<sup>52</sup> using  $T = -445 \times R2 + 641$ ,  
483 and that of Kouketsu et al.<sup>53</sup> using  $T = (-2.15 \times D1 - FWHM) + 478$  (see Supplementary Table  
484 1). Raman hyperspectral maps were obtained for selected areas within the thin sections 14-452-  
485 1B2 and 14-452-1B9, in streamspot mode (point-by-point scanning) using 1 x 6 s or 1 x 10 s  
486 exposures per point. Raman maps were generated using the software Wire 2.0 by selecting  
487 representative spectra for each component (minerals and kerogen) within the hyperspectral  
488 dataset (Fig. 3) and subsequent component analysis for each spectral point was determined  
489 using a background subtraction with a 2<sup>nd</sup> order polynomial fit. Maps of individual components  
490 were subsequently merged using the imaging program ImageJ.

491

492 **Carbon isotope analysis.** For isotope analysis of organic carbon, large rock samples (up to  
493 50x20 centimeters) were collected in the field from the freshest and least weathered outcrops  
494 available. In the lab all outer surfaces of the rocks were removed with a rock saw and were  
495 cut into smaller blocks, devoid of any cracks or fractures. Afterwards, mat horizons, 2 – 10 mm  
496 thick, were cut out individually with a thin rock saw and broken into smaller pieces, cleaned in  
497 an ultrasonic bath and dried. The resultant material was then crushed into a fine powder using  
498 an automated agate mill grinder, which was cleaned with pure quartz sand, distilled water, and  
499 ethanol between each run. The powders were decarbonated with 6N HCl for 12 hours then  
500 warmed at 80°C for 2h in a fume hood. Residues were rinsed with Milli-Q water, then  
501 centrifuged three to four times until they approached a neutral pH. 10 to 50 mg of decarbonated  
502 samples were loaded into tin capsule and analyzed for their carbon isotopic composition at the  
503 Pôle Spectrométrie Océan (PSO, Brest, France) using a Thermo Scientific Delta V plus mass  
504 spectrometer coupled to a Flash 2000 elemental analyzer. Isotopic results are reported in delta  
505 notation against the V-PDB standard (Vienna Pee Dee Belemnite) with an average analytical  
506 error of 0.12‰ (2σ, Supplementary Table 3). For C and O isotope composition of the mat-

507 associated carbonates, CO<sub>2</sub> was released from powdered samples by reaction with 100% H<sub>3</sub>PO<sub>4</sub>  
508 at 72°C in a Kiel IV automated carbonate preparation device. The CO<sub>2</sub> was analyzed using for  
509 isotope compositions using a Finnigan MAT 253 mass spectrometer. <sup>18</sup>O/<sup>16</sup>O and <sup>13</sup>C/<sup>12</sup>C ratios  
510 were also expressed in delta notation relative to the V-PDB standard (Supplementary Table 2).  
511 Precision for δ<sup>18</sup>O and δ<sup>13</sup>C<sub>carb</sub> was 0.2‰ (2σ) and 0.1‰ (2σ), respectively.

512

513 **Nitrogen isotope analysis.** Individual carbonaceous mat laminae were manually separated  
514 from fresh and unweathered sandstone samples (as described above), ground in an automated  
515 agate mill grinder, and sieved to ensure a grain size smaller than 140 μm. Bulk rock δ<sup>15</sup>N  
516 measurements were performed as they have been suggested to be more likely to record the  
517 primary isotopic composition of the original biomass in kerogen-poor greenschist-facies  
518 metasediments as compared to measurements of kerogen isolates<sup>54</sup>. To concentrate nitrogen in  
519 the insoluble residue, the samples were first decarbonated in HCl 6N for 12h overnight at room  
520 temperature, followed by 2h at 80°C in a fume hood. Residual material was rinsed three times  
521 with Milli-Q water, then centrifuged and dried at 50°C overnight. Approximately 500-1400 mg  
522 of powdered samples were analyzed following the method detailed in Ader et al.<sup>55</sup>.  
523 Conventional sealed tube combustion with CuO<sub>2</sub> and Cu rods (but in this study without CaO  
524 grains) was used to convert total nitrogen to N<sub>2</sub> (Dumas combustion), which was then purified  
525 using a secondary vacuum extraction line as shown in Figure 1 of Li et al.<sup>56</sup> N<sub>2</sub> nitrogen isotope  
526 ratio measurements were performed using a dual inlet Thermo-Fisher Delta V+ mass  
527 spectrometer at the IPGP in Paris (Supplementary Table 4). Each purified nitrogen gas sample  
528 was analyzed twice. Nitrogen blanks were lower than 0.1 micromoles, thus representing less  
529 than 10% of the measured nitrogen. External reproducibility of the δ<sup>15</sup>N<sub>sed</sub> measurements was  
530 ± 0.4 ‰ (1σ).

531

532 **Data availability.** The authors declare that all data supporting the study are available within  
533 the article and its Supplementary Information file.

534

## 535 **References**

- 536 51. Sforza, M. C., van Zuilen, M. A. & Philippot, P. Structural characterization by Raman  
537 hyperspectral mapping of organic carbon in the 3.46 billion-year-old Apex chert,  
538 Western Australia. *Geochim. Cosmochim. Acta* **124**, 18–33 (2014).
- 539 52. Beyssac, O., Goffé, B., Chopin, C. & Rouzaud, J. N. Raman spectra of carbonaceous  
540 material in metasediments: a new geothermometer. *J. Metamorph. Geol.* **20**, 859–871  
541 (2002).
- 542 53. Kouketsu, Y. *et al.* A new approach to develop the Raman carbonaceous material  
543 geothermometer for low-grade metamorphism using peak width. *Isl. Arc* **23**, 33–50  
544 (2014).
- 545 54. Stüeken, E. E., Zaloumis, J., Meixnerová, J. & Buick, R. Differential metamorphic  
546 effects on nitrogen isotopes in kerogen extracts and bulk rocks. *Geochim. Cosmochim.*  
547 *Acta* **217**, 80–94 (2017).
- 548 55. Ader, M., Boudou, J.-P., Javoy, M., Goffe, B. & Daniels, E. Isotope study on organic  
549 nitrogen of Westphalian anthracites from the Western Middle field of Pennsylvania  
550 (U.S.A.) and from the Bramsche Massif (Germany). *Org. Geochem.* **29**, 315–323  
551 (1998).
- 552 56. Li, L., Cartigny, P. & Ader, M. Kinetic nitrogen isotope fractionation associated with  
553 thermal decomposition of NH<sub>3</sub>: Experimental results and potential applications to trace  
554 the origin of N<sub>2</sub> in natural gas and hydrothermal systems. *Geochim. Cosmochim. Acta*  
555 **73**, 6282–6297 (2009).

557

558